

LETTER TO THE EDITOR

# The Kepler-11 system: evolution of the stellar high-energy emission and planetary initial atmospheric mass fractions

D. Kubyshkina<sup>1</sup>, L. Fossati<sup>1</sup>, A. J. Mustill<sup>2</sup>, P. E. Cubillos<sup>1</sup>, M. Davis<sup>2</sup>, N. V. Erkaev<sup>3,4</sup>, C. P. Johnstone<sup>5</sup>, K. G. Kislyakova<sup>5,1</sup>, H. Lammer<sup>1</sup>, M. Lendl<sup>1,6</sup>, and P. Odert<sup>1</sup>

<sup>1</sup> Space Research Institute, Austrian Academy of Sciences, Schmiedlstrasse 6, A-8042 Graz, Austria  
e-mail: [daria.kubyshkina@oeaw.ac.at](mailto:daria.kubyshkina@oeaw.ac.at)

<sup>2</sup> Lund Observatory, Department of Astronomy and Theoretical Physics, Lund University, Box 43, SE-221 00 Lund, Sweden

<sup>3</sup> Institute of Computational Modelling, FRC “Krasnoyarsk Science Center” SB RAS, “”, 660036, Krasnoyarsk, Russian Federation

<sup>4</sup> Siberian Federal University, 660041, Krasnoyarsk, Russian Federation

<sup>5</sup> Institute for Astronomy, University of Vienna, Türkenschanzstrasse 17, A-1180 Vienna, Austria

<sup>6</sup> Observatoire astronomique de l’Université de Genève 51 ch. des Maillettes, 1290 Sauverny, Switzerland

## ABSTRACT

The atmospheres of close-in planets are highly affected by mass loss driven by the stellar high-energy (X-ray and EUV) irradiation, in particular during the early stages of evolution. We recently developed a framework exploiting this connection and enabling to recover the past evolution of the stellar high-energy emission from the present-day properties of its planets. Furthermore, the framework can also provide constraints on planetary initial atmospheric mass fractions. The constraints on the output parameters improve when more planets can be simultaneously analysed, hence the Kepler-11 system, hosting six planets with bulk densities between 0.66 and 2.45 g cm<sup>-3</sup>, is an ideal target. We obtain that the star has likely evolved as a slow rotator (slower than 85% of the stars with similar masses), corresponding to a high-energy emission at 150 Myr ranging between 1 and 10 times that of the current Sun. We also constrain the planetary initial atmospheric mass fractions obtaining a 1–3% range, a lower limit of 3.5%, a 3–4.3% range, a 8.5–11% range, an upper limit of 15%, and a 4–7% range for planets b, c, d, e, f, and g, respectively. Our framework also suggests slightly higher masses for planets b, c, and f compared to what has been measured by transit timing variations. For planet g, we obtain a lower limit on planetary mass of  $\sim 10 M_{\oplus}$ . We coupled our results with published planet atmospheric accretion models obtaining a temperature and dispersal time of the protoplanetary disk of 550 K and 1 Myr, respectively, though these results may be affected by inconsistencies in the adopted system parameters. This work shows that our framework is capable of constraining important properties of planet formation models.

**Key words.** Hydrodynamics – Planets and satellites: atmospheres – Planets and satellites: physical evolution – Planets and satellites: individual: Kepler-11 b

## 1. Introduction

During the early stages of evolution, up to about 1–2 Gyr, late-type stars can follow different evolutionary paths in terms of their high-energy (X-ray + EUV: hereafter XUV) emission, hence rotation rate (e.g., Tu et al. 2015; Johnstone et al. 2015b). Furthermore, the XUV emission from young stars has a decisive impact on the atmospheric loss and evolution of their planets (e.g., Lopez & Fortney 2013; Owen & Lai 2018). Therefore, the present-day properties of planetary atmospheres are intimately related to the evolutionary path followed by their host stars.

Recently, we developed a framework making use of this connection to extract the evolutionary path of the stellar XUV emission. The framework uses a Bayesian scheme to track the evolution of a planetary atmosphere (i.e., track the evolution of the planetary radius) as a function of the stellar XUV flux evolution history considering the system parameters (planetary mass, orbital separation, stellar mass, current stellar rotation period, age of the system), their uncertainties, and fitting the currently observed planetary radius (Kubyshkina et al. 2019).

Within the framework of our model, the ideal objects to study are close-in sub-Neptune to Neptune-mass planets, as they are highly affected by atmospheric escape, and yet retain a sig-

nificant fraction of their primordial hydrogen-dominated atmosphere. In Kubyshkina et al. (2019), we tested the framework for a wide range of system parameters and then applied it to the HD 3167 and K2-32 planetary systems, each containing one planet with the appropriate characteristics for our analysis. However, tests we carried out and presented in that work, indicated that the constrain on the evolution of the stellar XUV flux may improve significantly when the analysis is carried out simultaneously considering multiple planet members of the same system.

With six rather low density sub-Neptune-like planets, the Kepler-11 system appears to be an ideal target for our framework. The Kepler-11 system is composed of six closely packed planets within 0.5 AU, with planetary radii in the range of 1.8 to 4.3  $R_{\oplus}$  but with a density range significantly smaller than that of planets of similar size in the Solar system. From an analysis of the first 16 months of Kepler photometry, Lissauer et al. (2011) derived the planetary radii from transits and masses from transit timing variations concluding that the five innermost Kepler-11 planets span a bulk density ranging between 0.5 and 3.0 g cm<sup>-3</sup>. Lissauer et al. (2013) revised the previous analysis employing 40 months of Kepler photometry obtaining slightly smaller planetary radii and significantly lower masses for the two innermost planets, reducing the range of bulk densities to

**Table 1.** Adopted planet parameters data for the Kepler-11 system.

planet	$d_0$ [au]	$M_{\text{pl}}[M_{\oplus}]$	$R_{\text{pl}}[R_{\oplus}]$	$\rho$ [ $\text{g cm}^{-3}$ ]	$f_{\text{at,now}}$ [%]
b	$0.091 \pm 0.001$ (a)	$2.78^{+0.64}_{-0.66}$ (a)	$1.83^{+0.07}_{-0.04}$ (a)	$2.45^{+0.63}_{-0.66}$ (a)	$0.043^{+0.035}_{-0.026}$ (b) $0.006^{+0.01}_{-0.005}$ (c)
c	$0.107 \pm 0.001$ (a)	$5.00^{+1.30}_{-1.35}$ (a)	$2.89^{+0.12}_{-0.04}$ (a)	$1.11^{+0.32}_{-0.32}$ (a)	$1.52^{+0.34}_{-0.30}$ (b) $0.95^{+0.44}_{-0.41}$ (c)
d	$0.155 \pm 0.001$ (a)	$8.13^{+0.67}_{-0.66}$ (a)	$3.21^{+0.12}_{-0.04}$ (a)	$1.33^{+0.14}_{-0.15}$ (a)	$3.33^{+0.28}_{-0.26}$ (b) $2.72^{+0.29}_{-0.27}$ (c)
e	$0.195 \pm 0.002$ (a)	$9.48^{+0.86}_{-0.88}$ (a)	$4.26^{+0.16}_{-0.07}$ (a)	$0.66^{+0.08}_{-0.09}$ (a)	$9.39^{+0.78}_{-0.73}$ (b) $6.97^{+0.57}_{-0.55}$ (c)
f	$0.250 \pm 0.002$ (a)	$2.53^{+0.49}_{-0.45}$ (a)	$2.54^{+0.10}_{-0.04}$ (a)	$0.83^{+0.18}_{-0.16}$ (a)	$1.21^{+0.21}_{-0.18}$ (b) $0.91^{+0.30}_{-0.26}$ (c)
g	$0.466 \pm 0.004$ (a)	< 27 (a)	$3.33^{+0.26}_{-0.09}$ (a)	< 45 (a)	–

**Notes.**  $f_{\text{at,now}}$  is the current atmospheric mass fraction; (a) – Bedell et al. (2017); (b) – based on Lopez & Fortney (2014); (c) – based on Johnstone et al. (2015a)

$0.6\text{--}1.7 \text{ g cm}^{-3}$ . In both studies, the stellar properties were obtained from the analysis of one (Lissauer et al. 2011) or two (Lissauer et al. 2013) Keck I spectra analysed with Spectroscopy Made Easy (Valenti & Piskunov 1996; Valenti & Fischer 2005). From comparisons of the spectroscopic analysis results with stellar evolutionary tracks, they finally adopted a stellar mass of  $0.961 \pm 0.025 M_{\odot}$  and an age of  $8.5^{+1.1}_{-1.4}$  Gyr.

Bedell et al. (2017) revised the stellar properties using 22 newly obtained Keck spectra finally deriving a stellar mass of  $1.042 \pm 0.005 M_{\odot}$  and a system age of  $3.2 \pm 1.5$  Gyr, indicating that Kepler-11 is very similar to the Sun. In addition to comparisons with stellar evolutionary tracks, Bedell et al. (2017) inferred the age of the system employing gyrochronology (obtaining an age of 3–3.4 Gyr), lithium abundance (obtaining an age of  $3.5 \pm 1.0$  Gyr), the Yttrium-to-Magnesium [Y/Mg] abundance ratio (obtaining an age of  $4.0 \pm 0.7$  Gyr), and stellar activity (obtaining an age of  $\sim 1.7$  Gyr). All these estimates are well below those of Lissauer et al. (2013). By changing the stellar properties, Bedell et al. (2017) revised also the planetary properties obtaining somewhat different masses compared to previous estimates, however the bulk densities changed only slightly. Planetary masses, radii, and bulk densities obtained by Bedell et al. (2017) are listed in Table 1.

We present here the results obtained from simultaneously modelling the atmospheric evolution of all Kepler-11 planets considering the more recent parameters given by Bedell et al. (2017). We also describe here a few upgrades to modelling framework described by Kubyshkina et al. (2019). We give constraints on the evolution of the XUV emission of the host star and on the initial atmospheric mass fraction of the Kepler-11 planets. This paper is organised as follows. Section 2 gives a brief description of the modelling framework and of its upgrade with respect to what described in Kubyshkina et al. (2019). Sections 3 and 4 present the results and their discussion, while Section 5 draws the conclusions of this work.

## 2. Modeling approach

The modelling framework used for the analysis of the Kepler-11 system is the one developed and thoroughly described in Kubyshkina et al. (2019), but with a few improvements that we detail here below. The modelling approach combines three main ingredients necessary to study the evolution of a planetary atmo-

sphere: a model of the stellar flux evolutionary track, a model relating planetary parameters and atmospheric mass, and a model computing atmospheric escape rates.

The amount of XUV flux emitted by a late-type star is tightly related to the stellar rotation rate, and the evolutionary tracks for the stellar rotation rate of young ( $\lesssim 2$  Gyr) late-type stars may follow different paths ranging from slow (rotation period longer than 8 days) to fast (rotation period shorter than 3 days) rotation (Johnstone et al. 2015b; Tu et al. 2015). To account for this, we model the rotation period (in days) as a power law in  $\tau$  (age), normalised such that the rotation period at the present age ( $T_{\text{age}}$ ) is consistent with the measured stellar rotation period ( $P_{\text{rot}}^{\text{now}}$ ), obtaining

$$P_{\text{rot}} = \begin{cases} P_{\text{rot}}^{\text{now}} \left( \frac{\tau}{T_{\text{age}}} \right)^{0.566}, & \tau \geq 2 \text{ Gyr} \\ P_{\text{rot}}^{\text{now}} \left( \frac{2 \text{ Gyr}}{T_{\text{age}} [\text{Gyr}]} \right)^{0.566} \left( \frac{\tau [\text{Gyr}]}{2 \text{ Gyr}} \right)^x, & \tau < 2 \text{ Gyr} \end{cases} \quad (1)$$

where the exponent  $x$  is a positive value, typically ranging between 0 and  $\sim 2$ , controlling the stellar rotation period at ages younger than 2 Gyr. After 2 Gyr, the different paths converge into one, for which we take the empirical power law given by Mamajek & Hillenbrand (2008).

From the rotation period at each moment in time, we derive the stellar X-ray and EUV luminosities following Pizzolato et al. (2003) and Wright et al. (2011), that relate rotation rates and stellar masses to X-ray luminosity, including saturation effects for the fastest rotators, and Sanz-Forcada et al. (2011), relating X-ray and EUV fluxes. To account for variations of the stellar bolometric luminosity, hence of the planetary equilibrium temperature, with time, we use the MESA Isochrones and Stellar Tracks (MIST, Paxton et al. 2018) model grid.

To estimate the planetary mass-loss rate at each moment in time from the stellar flux and planetary parameters (mass  $M_{\text{pl}}$ , radius  $R_{\text{pl}}$ , equilibrium temperature  $T_{\text{eq}}$ , and orbital separation  $d_0$ ), we use the analytic formulas given by Kubyshkina et al. (2018b), which have been derived fitting the results of a large grid of one-dimensional hydrodynamic upper-atmosphere models for planets hosting a hydrogen-dominated atmosphere (Kubyshkina et al. 2018a).

To estimate the atmospheric mass of a planet  $M_{\text{atm}}$  as a function of planetary parameters, in Kubyshkina et al. (2019) we employed the results of the model presented by Johnstone et

al. (2015a), pre-computing a grid of atmospheric masses for the range of planetary parameters covered by Kubyshkina et al. (2018a,b), among which we further interpolate during an evolution run. However, a series of works studying the Kepler-11 system (including Lissauer et al. 2011, 2013; Ikoma & Hori 2012) used the approximation given by Lopez & Fortney (2013, 2014). For this reason, to enable comparisons between our and previous results, particularly with respect to the initial atmospheric mass fraction  $f_{\text{at},0}$ , in the present work we employ the approximation of Lopez & Fortney (2014) as prime tool for deriving atmospheric mass fractions from the system parameters. However, we compared the two approaches for the specific case of the Kepler-11 system obtaining that the approximation of Lopez & Fortney (2014) leads to slightly higher atmospheric mass than the model by Johnstone et al. (2015a), with differences increasing with planetary mass and reaching about 7% for planet e. We further tested the dependence of the final results on this choice finding that the differences are not significant.

In our previous works modelling planetary atmospheric evolution (Kubyshkina et al. 2018a, 2019), we considered an initial planetary radius (and therefore  $f_{\text{at},0}$ ) corresponding to a value of the restricted Jeans escape parameter  $\Lambda$  equal to 5, where  $\Lambda$  is the Jeans escape parameter at the position of the planetary radius and for a temperature equal to  $T_{\text{eq}}$ , for a hydrogen-dominated atmosphere (Jeans 1925; Fossati et al. 2017). As we showed in Kubyshkina et al. (2019), this approximation does not influence the result for the majority of planets, but some of the planets in the Kepler-11 system (d, e and likely g) are an exception. Therefore, in this work we further set the initial atmospheric mass fraction of all planets as a free parameter.

Combining the ingredients described above enables us computing planetary atmospheric evolutionary tracks for any set of input parameters. We assume that stellar mass remains constant with time and ignore the contribution of gravitational contraction and radioactive decay on  $T_{\text{eq}}$  during the first phases of evolution. We further assume that each planet accreted a hydrogen-dominated atmosphere from the proto-planetary nebula. The starting time of the simulations is set to 5 Myr, which is the typical lifetimes of protoplanetary disks (Mamajek 2009), but we run tests for starting ages ranging between 0.3 and 10 Myr (see Section 3).

The analysis in this paper relies on the assumption that the orbital semimajor axes of the Kepler-11 planets have remained roughly constant since the dispersal of the gas disc. We now justify this assumption, arguing that only a very minor change in semimajor axes of a few percent can have taken place: a strong instability in the system's past is unlikely, but tidal forces may have caused a minor change in semimajor axes.

Using the parameters of Lissauer et al. (2013), the inner 5 planets are separated by 9.1, 16.6, 9.1 and 11.5 mutual Hill radii, while orbital eccentricities are low ( $< 0.05$ ) and the system is coplanar to within  $1^\circ$ . Such a compact, dynamically cold configuration likely rules out any significant orbital changes since the epoch of planet formation, which must have occurred within the gas disc for the planets to have acquired their significant hydrogen envelopes. The high multiplicity, low eccentricities and inclinations, and near-resonant period ratios are characteristic of super-Earth systems that remain stable after formation in the gas disc (Izidoro et al. 2019; Lambrechts et al. 2019). Further support for dynamical stability of the system comes from Lissauer et al. (2013), who showed that the best fit for the system is stable for at least 250 Myr. They also showed that assigning higher eccentricities resulted in instability on a much shorter

timescale ( $\sim 1$  Myr), further favouring a dynamically cold configuration (low eccentricity and inclination).

Although the planets have likely not undergone any major orbital changes since their formation, a small change in their semi-major axes could have occurred as a result of tidal deformation of the planets. Using the constant- $Q$  tidal model of Jackson et al. (2008), and assuming a planetary tidal quality factor  $Q'_{\text{pl}}$  of 100, we find a timescale for tidal eccentricity damping of the inner planet of  $\sim 400$  Myr, so some tidal evolution in the system is certainly possible. Kepler-11b and c are just wide of the 5:4 mean motion resonance, and differential tidal dissipation of neighbouring resonant planets has been invoked to explain why many Kepler systems have orbital period ratios just wide of exact integer ratios (e.g., Delisle et al. 2014; Delisle, & Laskar 2014). In such scenarios, the orbital semi-major axes change by only a few percent, as the damping ceases once the planets move away from the resonance and the associated eccentricity forcing weakens. Such a small change in orbital semi-major axes will result in a similarly small change in the incident XUV flux on the planets, much smaller than the range of fluxes corresponding to the range of stellar rotation histories considered in this paper.

At each step of the evolution, first we compute the mass-loss rate based on the stellar flux and system parameters, which we use to update the atmospheric mass fraction, and the planetary radius. We adjust the time step, such that the change in atmospheric mass  $M_{\text{atm}}$  is less than 5%.

Finally, we apply a Bayesian approach to constrain the planetary initial mass fractions and the evolutionary tracks of the stellar XUV luminosity fitting the currently observed planetary radii. To this end, we combine the planetary evolution model with the open-source Markov-chain Monte Carlo (MCMC) algorithm of Cubillos et al. (2017), to compute the posterior distributions for  $f_{\text{at},0}$  for each planet, the stellar rotation rate, and the considered system parameters.

For each MCMC run, we let the planetary masses, age of the system, present-time rotation period, orbital separations, and stellar mass as free parameters, with Gaussian-like priors according to the measured values and uncertainties. For those parameters which are not known (initial atmospheric masses and the power law  $x$  in Equation (1), which sets the evolution of the stellar XUV luminosity), we set a uniform prior within the following ranges. For  $x$ , we consider a range from 0 to 2, where 0 corresponds to the stellar rotation period remaining constant before 2 Gyr and 2 corresponds to periods shorter than 0.3 days for the parameters of Kepler-11. For the atmospheric mass fractions of the five inner planets, we set uniform priors from 0 to 30%, while for the possibly heavier planet g, we set a uniform prior between 0 and 100%. Increasing the upper limit for the atmospheric mass fractions does not significantly affect the results.

As the degree of the power law  $x$  given in Equation (1) is not intuitively clear, we provide the results in terms of the stellar rotation period at the age of 150 Myr. This particular age was chosen, as it allows comparing with the distribution of stellar rotation periods measured in young open clusters (Johnstone et al. 2015b).

### 3. Results

As mentioned above, we consider the system parameters given by Bedell et al. (2017). We obtain a rotation period at 150 Myr ranging between 6.3 and 19.7 days (Figure 1, top left panel), which corresponds to the long period wing of the distribution obtained for stars in  $\approx 150$  Myr old open clusters (Johnstone et

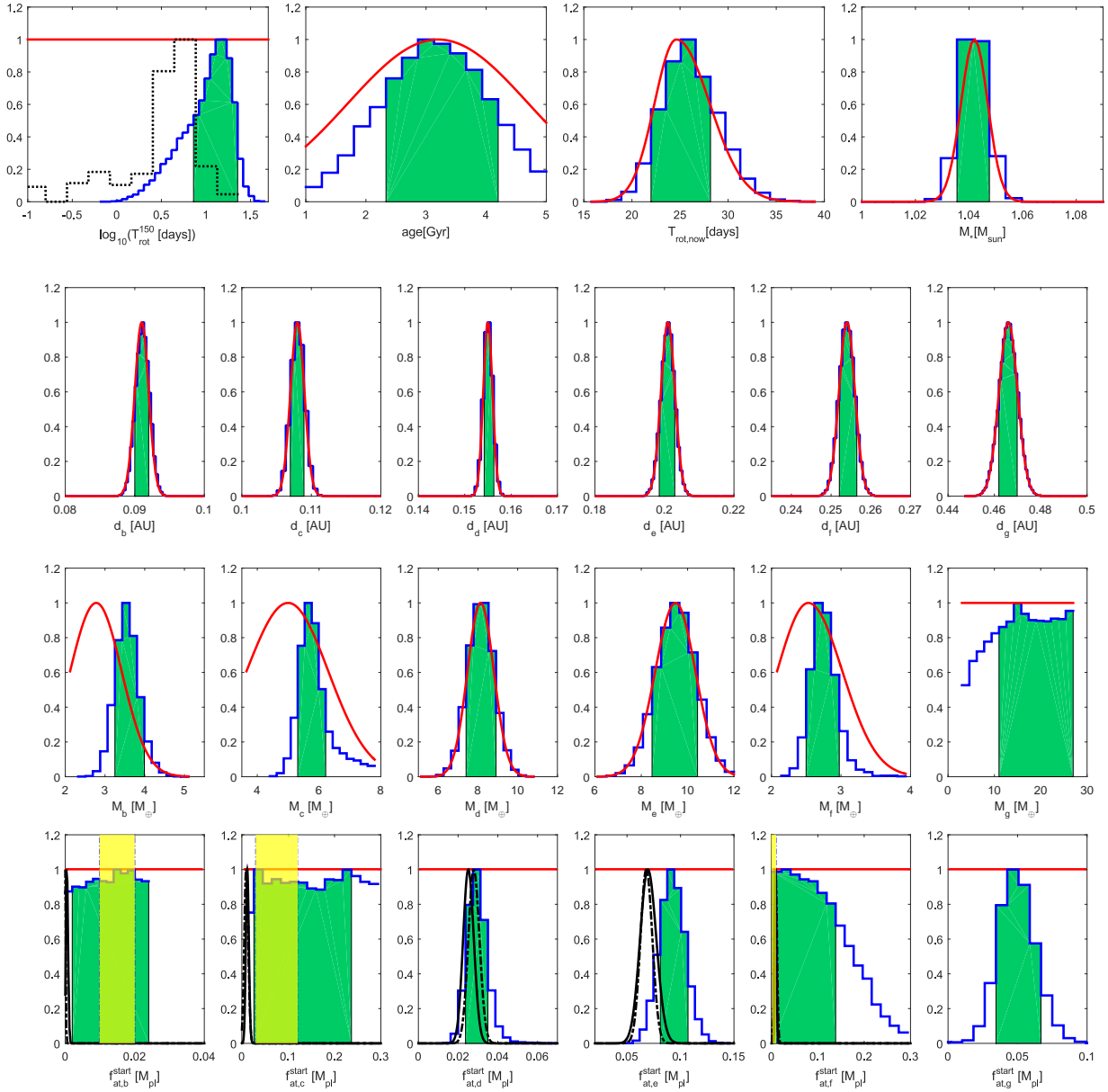


**Fig. 1.** Posterior probabilities for the considered Kepler-11 system parameters. Top row – stellar parameters, from left to the right: rotation period at an age of 150 Myr, age of the system, present time stellar rotation period, and stellar mass. Second row – planet orbital distance ( $d$ ). Third row – planetary mass. Bottom row – initial atmospheric mass fraction (i.e., at an age of 5 Myr). The blue solid lines indicate the posterior probabilities, the green shaded areas correspond to the 68% HPD credible intervals, and the red solid lines are the priors. The dashed magenta line in the top-left panel shows the distribution measured for solar mass stars member of  $\approx 150$  Myr-old open clusters (Johnstone et al. 2015b). The black lines in the bottom row illustrate the present time atmospheric mass fractions obtained using the approximation given by Lopez & Fortney (2014, solid line) or the model of Johnstone et al. (2015a, dashed line). The yellow shaded areas in the bottom row are the initial atmospheric mass fractions given by the accretion models of Ikoma & Hori (2012) for a disk temperature of 550 K and a disk dispersal time of 1 Myr (see text).

al. 2015b). In terms of X-ray luminosity, this range corresponds to values ranging between about 1 and 10 times the X-ray luminosity of the present Sun.

The posterior distributions of the system parameters are consistent with the priors, except for the mass of planet b, for which the posterior peaks at the  $1\sigma$  upper boundary of the prior. The planet lies very close to the host star, making it subject to powerful escape. For this reason, since planet b is likely to still host a shallow hydrogen-dominated atmosphere (see Table 1), to avoid complete atmospheric escape the framework tends to increase

the mass of the planet, as discussed in detail in Kubyshkina et al. (2019).

Excluding planet g, for which the prior mass is unconstrained, for the heavier planets in the system (i.e., d and e) the mass posteriors match well the prior distributions, while for the lighter planets (b, c, and f) the posteriors are significantly narrower than the priors. In fact, the 68% higher posterior density (HPD) credible intervals are  $3.25\text{--}4.00 M_{\oplus}$ ,  $5.30\text{--}6.21 M_{\oplus}$ , and  $2.46\text{--}2.92 M_{\oplus}$  for planets b, c, and f, respectively. When setting the starting time of the simulations below 3 Myr, the mass posterior of planet b shifts further towards higher values as the

algorithm tries in this way to prevent a complete escape of the atmosphere. For planet g, the posterior distribution has a local maximum around  $15 M_{\oplus}$ , is almost uniform above this value, and decreases steeply below  $10 M_{\oplus}$ . This allows us just to set a lower limit of  $10 M_{\oplus}$  on the planetary mass.

The  $f_{\text{at},0}$  posterior distributions (bottom row of Figure 1) are close to uniform for the two innermost planets, but are well constrained for planets d, e, f, and g. For planets b and c, we respectively obtain an upper and a lower limit of 3 and 3.5%. For planet f, the least massive in the system, the posterior probability distribution is almost flat up to 10% (with a peak at 3%) and decreases steeply above this. The posterior distributions for planets d and e have a Gaussian-like shape with the HDP credible intervals lying in the 3–4.3 and 8.5–11% ranges, respectively. From the  $f_{\text{at},0}$  posterior distributions we conclude that the atmospheres of the two heavier planets (d and e) likely remained nearly unaffected by atmospheric escape, while the lighter planets b, c, and f have lost a significant amount of hydrogen, up to more than 10 times the present day atmospheres.

#### 4. Discussions

Based on the system parameters given by Lissauer et al. (2011), Ikoma & Hori (2012) studied atmospheric accretion within the nebula for the five inner planets assuming a range of temperatures for the protoplanetary disk ranging between 200 and 940 K and disk dispersal ages ranging between 0.01 and 10 Myr. Therefore, the work of Ikoma & Hori (2012) provides a way to use the planetary atmospheric mass fractions derived above to infer properties of the protoplanetary disk.

The model of Ikoma & Hori (2012) assumes the presence of a grainless atmosphere with a solar H/He abundance on top of a rocky body<sup>1</sup> in pressure balance with the protoplanetary disk at the smaller between the Bondy and Hill spheres (setting the upper boundary density and temperature) and heated by the rocky core from below. They assume that at the beginning of the simulation the planet is hot, but has no further energy supply, so the rocky body cools rapidly, on a time scale much shorter than the atmospheric accretion time scale. The protoplanetary disk dissipates concurrently with the growth of the atmosphere until full dissipation. The decrease of the disk density results in atmospheric cooling. Furthermore, during disk dissipation, the atmospheres of planets with masses too low to undergo runaway accretion experience significant erosion due to the expansion of the atmosphere as a consequence of the decreasing external pressure provided by the disk (Stökl et al. 2015; Owen & Wu 2017). Because of their low mass, this applies also to the planets in the Kepler-11 system.

A direct combination of our and Ikoma & Hori (2012)'s results is not strictly possible because of differences in the considered planetary and stellar masses, however the masses of planets d and e did not change significantly between Lissauer et al. (2011), considered by Ikoma & Hori (2012), and Bedell et al. (2017) considered here. For this reason, we looked for the parameters of the protoplanetary disk in the work of Ikoma & Hori (2012) best fitting the mass and  $f_{\text{at},0}$  posterior distributions of planets d and e obtaining a disk dispersal time of 1 Myr and a temperature of 550 K. Having then fixed the disk dispersal time and temperature with the results on planets d and e, we looked for the range of atmospheric mass fractions predicted by Ikoma & Hori (2012) for planets b, c, and f corresponding to the range of planetary masses given by our probability distributions for

these three planets. We obtained  $f_{\text{at},0}$  values in the following ranges:  $\sim 1$ –2% for the planet b,  $\sim 3$ –12% for the planet c, and below 0.5% for the planet f (see yellow shaded areas in Figure 1). These ranges agree well with our estimates, except for planet f where the range is at the lower boundary of our HPD credible interval and it actually partly lies even below the present time atmospheric mass fraction. Such a small value of initial atmospheric mass fraction seems unlikely, possibly suggesting that the protoplanetary disk may have survived slightly longer than 1 Myr. These results indicate that our analysis has the potential to provide important constraints to planet formation models and calls for dedicated formation models more consistent with our input parameters and assumptions.

Figure 2 presents the pair-wise posterior distributions of the system parameters. In total, each MCMC run includes 22 parameters, but, to improve the readability of the plot, we excluded stellar mass and planetary orbital separations, as they match the priors and do not show any correlation with other parameters. We inspected Figure 2 searching for correlations. There is a weak correlation between age of the system and stellar rotation period at 150 Myr  $P_{150}$ , where a younger star corresponds to a slower rotator. The masses of planets b, c, and f are also correlated with  $P_{150}$  (slower the rotator lighter the planet) and age of the system (younger the system lighter the planet). The initial atmospheric mass fractions of planets d, e, and g present a weak correlation with age (younger the system smaller the initial envelope). The initial atmospheric mass fractions of planets b and c, instead, are independent of both age and stellar rotation period, indicating that the evolution of these atmospheres is completely set in the first few Myrs during the saturation phase of the stellar XUV emission. These correlations arise because the strength and extent of atmospheric escape, hence the evolution of the planetary radius, depends on the age of the system, planetary mass, and stellar XUV emission, which is tightly related to the stellar rotation period (Section 2).

#### 5. Conclusions

The Kepler-11 system is composed by an approximately solar mass star and six planets in the super-Earth to Neptune mass range, five of which orbiting within the distance of Mercury to the Sun. Yet, all Kepler-11 planets seem to still retain a hydrogen-dominated atmosphere. We employed a planetary atmospheric evolution scheme in a Bayesian framework to derive the evolutionary path of the stellar rotation period, hence high-energy emission, and to constrain the initial mass fractions of the six planets.

Our results indicate that such an exotic configuration with six close-in, low-density planets is possible if the star has evolved as a slow rotator, following an evolution of the rotation period covered by about 15% of all stars in the 0.9–1.1  $M_{\odot}$  mass range. We also found that the initial atmospheric mass fractions can be well constrained for heavy and/or distant planets, because for such planets atmospheric escape is not strong enough to dramatically affect the atmosphere, even during the early stages of evolution. Specifically, in the Kepler-11 system, this is the case of planets d and e, for which we obtain narrow posterior distributions of the initial atmospheric mass fraction, which indicate that both planets have lost about 30% of their initial hydrogen atmospheric content. In particular, for planets d and e, we find that the initial atmospheric mass fraction was likely to lie within 3–4.3 and 8.5–11%, respectively. For the outermost planet (planet g), assuming a  $15 M_{\oplus}$ , which corresponds to the peak of our posterior distribution, escape has led to a total loss of about 10% of the initial

<sup>1</sup> The density of the rocky core has a minor impact on the result.

hydrogen atmospheric content, with an initial atmospheric mass fraction peaking at about 5%. For the other planets in the system (b, c, and f), the probability distributions of the initial mass fraction are significantly broader, but still enable us to put some constrain. For planet b, we find that the initial atmospheric mass fraction was smaller than 3%, for planet c we find that it was larger than 3.5%, while for planet f we find that it was smaller than 15%.

We further employed our results for planets d and e in combination with those of Ikoma & Hori (2012) to make a first attempt constraining the temperature and lifetime of the protoplanetary disk obtaining values of 550 K and 1 Myr, respectively. Further comparisons for planets b, c, and f suggest that a disk dispersal time of 1 Myr may be underestimated. We remark that these results shall, however, be taken with caution because of differences in the system parameters considered in this work and by Ikoma & Hori (2012).

We have shown that planetary atmospheric evolution modelling can be a very powerful tool for constraining both planet formation processes and stellar characteristics that would be otherwise difficult, if not impossible, to obtain. The only drawback of our analysis framework is that it is effective only for systems hosting at least one planet currently holding a hydrogen-dominated atmosphere and for which the planetary mass and age of the system are well measured. Most (sub-)Neptunes have so far been detected by the Kepler and K2 missions, but for many of these planets masses (and typically also ages) are poorly constrained. The TESS and CHEOPS missions are expected to greatly increase the number of systems on which our analysis will be possible and effective, hence giving us the possibility to constrain planet formation and the evolution of stellar rotation on the basis of a statistically significant sample of planets.

## References

- Bedell, M., Bean, J. L., Meléndez, J., et al. 2017, *ApJ*, 839, 94  
Cubillos, P., Harrington, J., Loredó, T. J., et al. 2017, *AJ*, 153, 3  
Delisle, J.-B., Laskar, J., & Correia, A. C. M. 2014, *A&A*, 566, A137  
Delisle, J.-B., & Laskar, J. 2014, *A&A*, 570, L7  
Fossati, L., Erkaev, N. V., Lammer, H., et al. 2017, *A&A*, 598, A90  
Ikoma, M., & Hori, Y. 2012, *ApJ*, 753, 66  
Izidoro, A., Bitsch, B., Raymond, S. N., et al. 2019, arXiv e-prints, arXiv:1902.08772  
Jackson, B., Greenberg, R., & Barnes, R. 2008, *ApJ*, 678, 1396  
Jeans, J. 1925, *The Dynamical Theory of Gases*. By Sir James Jeans. Cambridge University Press, 1925. ISBN: 978-1-1080-0564-7  
Johnstone, C. P., Güdel, M., Stökl, A., et al. 2015a, *ApJ*, 815, L12  
Johnstone, C. P., Güdel, M., Brott, I., & Lüftinger, T. 2015b, *A&A*, 577, A28  
Kubyschkina, D., Cubillos, P., Fossati, L., et al. 2019, *ApJ*, 879, 1, 26  
Kubyschkina, D., Fossati, L., Erkaev, N. V., et al. 2018a, *A&A*, 619, A151  
Kubyschkina, D., Fossati, L., Erkaev, N. V., et al. 2018b, *ApJ*, 866, L18  
Lambrechts, M., Morbidelli, A., Jacobson, S. A., et al. 2019, *A&A*, 627, A83  
Lissauer, J. J., Fabrycky, D. C., Ford, E. B., et al. 2011, *Nature*, 470, 53  
Lissauer, J. J., Jontof-Hutter, D., Rowe, J. F., et al. 2013, *ApJ*, 770, 131  
Lopez, E. D., & Fortney, J. J. 2013, *ApJ*, 776, 2  
Lopez, E. D., & Fortney, J. J. 2014, *ApJ*, 792, 1  
Mamajek, E. E., & Hillenbrand, L. A. 2008, *ApJ*, 687, 1264-1293  
Mamajek, E. E. 2009, *American Institute of Physics Conference Series*, 1158, 3  
Owen, J. E., & Wu, Y. 2017, *ApJ*, 847, 29  
Owen, J. E., & Lai, D. 2018, *MNRAS*, 479, 5012  
Paxton, B., Schwab, J., Bauer, E. B., et al. 2018, *ApJS*, 234, 34  
Pizzolato, N., Maggio, A., Micela, G., Sciortino, S., & Ventura, P. 2003, *A&A*, 397, 147  
Sanz-Forcada, J., Micela, G., Ribas, I., et al. 2011, *A&A*, 532, A6  
Stökl, A., Dorfi, E., & Lammer, H. 2015, *A&A*, 576, A87  
Tu, L., Johnstone, C. P., Güdel, M., & Lammer, H. 2015, *A&A*, 577, L3  
Valenti, J. A., & Fischer, D. A. 2005, *ApJS*, 159, 141  
Valenti, J. A., & Piskunov, N. 1996, *A&AS*, 118, 595  
Wright, N. J., Drake, J. J., Mamajek, E. E., & Henry, G. W. 2011, *ApJ*, 743, 48

*Acknowledgements.* We acknowledge the Austrian Forschungsförderungsgesellschaft FFG project “TAPAS4CHEOPS” P853993, the Austrian Science Fund (FWF) NFN project S11607-N16, and the FWF project P27256-N27. NVE acknowledges support by the RFBR grant No. 15-05-00879-a and 16-52-14006 ANF\_a.

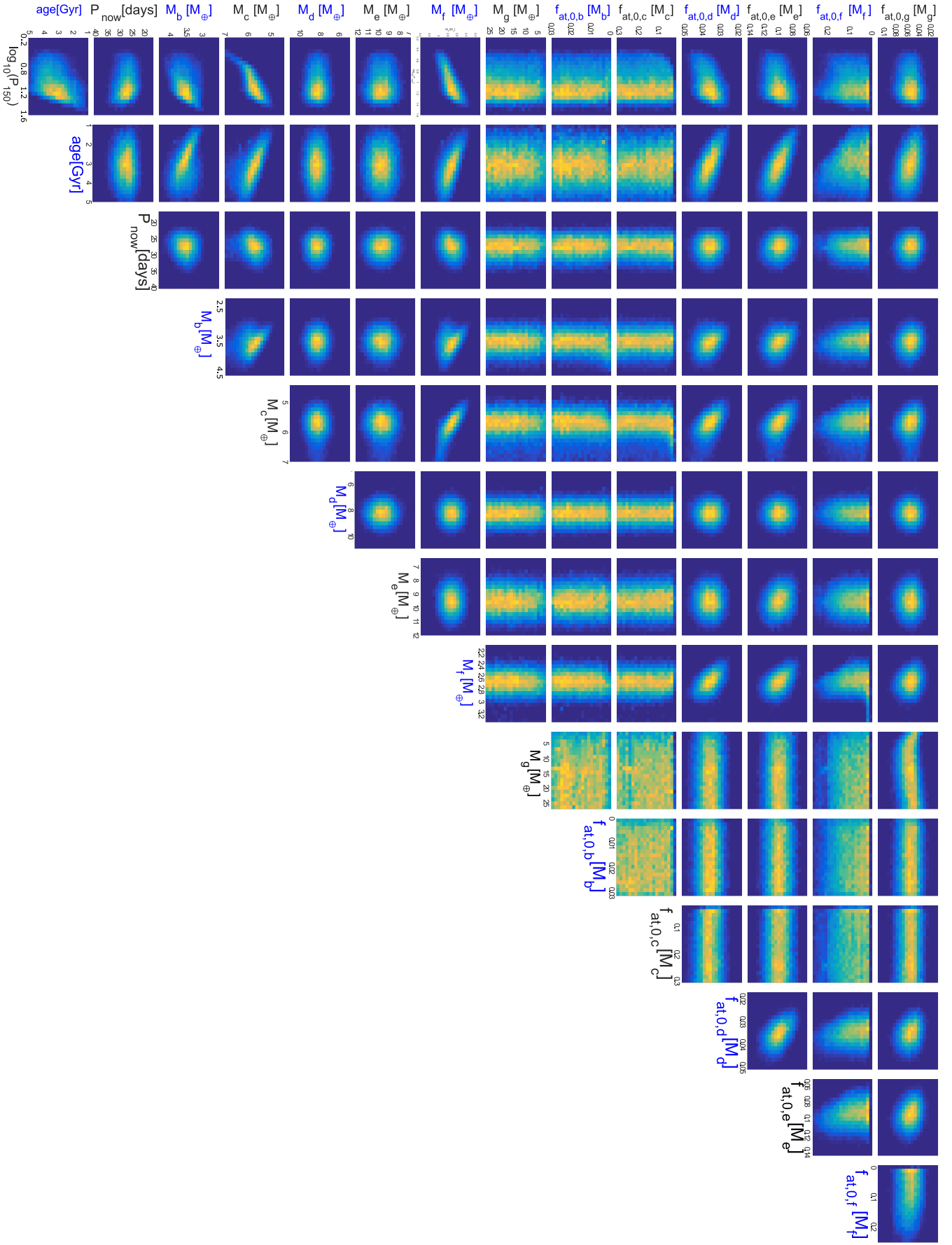


Fig. 2. Pair-wise distributions of the most relevant system parameters.